

Discovery of a biofilm electrocline using real-time 3D metabolite analysis

Dipankar Koley^{a,1}, Matthew M. Ramsey^{b,1}, Allen J. Bard^{a,2}, and Marvin Whiteley^{b,c,2}

^aCenter for Electrochemistry, Department of Chemistry and Biochemistry, ^bSection of Molecular Genetics and Microbiology, and ^cInstitute for Cellular and Molecular Biology, University of Texas, Austin, TX 78712

Contributed by Allen J. Bard, October 28, 2011 (sent for review August 30, 2011)

Bacteria are social organisms that possess multiple pathways for sensing and responding to small molecules produced by other microbes. Most bacteria in nature exist in sessile communities called biofilms, and the ability of biofilm bacteria to sense and respond to small molecule signals and cues produced by neighboring biofilm bacteria is particularly important. To understand microbial interactions between biofilms, it is necessary to perform rapid, real-time spatial quantification of small molecules in micro-environments immediately surrounding biofilms; however, such measurements have been elusive. In this study, scanning electrochemical microscopy was used to quantify small molecules surrounding a biofilm in 3D space. Measuring concentrations of the redox-active signaling molecule pyocyanin (PYO) produced by biofilms of the bacterium *Pseudomonas aeruginosa* revealed a high concentration of PYO that is actively maintained in the reduced state proximal to the biofilm. This gradient results in a reduced layer of PYO that we have termed the PYO “electrocline,” a gradient of redox potential, which extends several hundred microns from the biofilm surface. We also demonstrate that the PYO electrocline is formed under electron acceptor-limiting conditions, and that growth conditions favoring formation of the PYO electrocline correlate to an increase in soluble iron. Additionally, we have taken a “reactive image” of a biofilm surface, demonstrating the rate of bacterial redox activity across a 2D surface. These studies establish methodology for spatially coordinated concentration and redox status measurements of microbe-produced small molecules and provide exciting insights into the roles these molecules play in microbial competition and nutrient acquisition.

ultramicroelectrode | square wave voltammetry | local redox microenvironment | reduced pyocyanin layer

Bacteria possess the ability to sense a wide-range of microbe-produced extracellular small molecules and respond through modulation of specific behaviors. Some extracellular small molecules serve as dedicated signals that have evolved to permit microorganisms to communicate both with self (same species or strain) and nonself cells (1). Such signals allow a bacterial community to coordinate its behavior based on local cell density and mass transfer of the surrounding environment, a process referred to as quorum sensing (QS) (2). Other small molecules serve as chemical cues that provide information to a recipient microbe, but differ from a signal in that they did not evolve explicitly for that purpose (1). Cues are chemically and functionally diverse and include primary metabolites arising from central metabolism as well as secondary metabolites. Although dedicated signals have been the focus of significant research over the last 20 y, it is clear that primary and secondary metabolites also impact the species composition and behaviors of microbial communities *in vitro* and *in vivo* (3–5). In some cases, once-presumed dedicated signals have been shown to also act as cues, suggesting that many small molecules may be multifunctional (1, 6–8).

Both bacterial signals and cues are structurally diverse but, in general, are small molecular mass (<1,000 Da) and synthesized from central metabolites. The responses to such molecules are also diverse, including but not limited to: biosynthesis of

antimicrobials (9–12), production of light (13, 14), colonization and proliferation within disease sites (4, 15), and resistance to killing by the innate immune system (5). As with many microbiological studies, elucidation of the molecular details of signal/cue synthesis and response has been performed by using bacteria grown in homogenous planktonic (free-swimming) populations. Although such studies have provided detailed insight into synthesis and response of these small molecules, bacteria in nature often do not exist in high-density planktonic communities. Instead, natural bacterial populations often exist in high-density, low-cell number biofilm communities (16). A biofilm is a bacterial community attached to a surface, or to each other, and surrounded by an extracellular polymeric matrix. Biofilms are distinct from well-mixed planktonic cultures in that they are spatially heterogeneous, both in regard to chemical gradients and bacterial phenotypes (17, 18). This heterogeneity has been proposed to have important biological consequences by producing a diverse community better able to resist external stresses, a phenomenon termed the “insurance hypothesis” (19).

Numerous technological advancements have allowed for the examination of chemical gradients within biofilms, primarily through the use of *in situ* responsive fluorophores or microprobes (20–23). However, a fundamental question still exists regarding the nature of such gradients in bulk solution surrounding a biofilm. This question is important because these gradients are likely critical for determining how spatially separated bacteria communities sense and respond to neighboring communities. The primary challenge to these experiments is the ability to quantify and spatially resolve small molecules immediately surrounding biofilms in real-time. In a previous study (24), our laboratories have begun to address the challenge of spatial metabolite profiling through the use of scanning electrochemical microscopy (SECM) to quantify a primary metabolite produced by a bacterial biofilm in real-time. SECM has the unique ability to set the exact distance from an ultramicroelectrode sensing tip to a biological substrate through a feedback approach curve (25) and, thus, is able to measure the local concentration of redox active small molecules over a biofilm. SECM also has the ability to scan over a substrate in the *x-y* direction, providing a spatial concentration profile over the surface.

In this study, we used SECM to interrogate production of the QS-controlled, redox-active secondary metabolite pyocyanin (PYO) produced by biofilms of the pathogenic bacterium *Pseudomonas aeruginosa*. PYO was chosen for study because it is a multifunctional molecule, serving both as a QS signal (26), a potent antimicrobial *in vitro* and *in situ* (3, 27), and as

Author contributions: D.K., M.M.R., A.J.B., and M.W. designed research; D.K. and M.M.R. performed research; D.K., M.M.R., A.J.B., and M.W. analyzed data; and D.K., M.M.R., A.J.B., and M.W. wrote the paper.

The authors declare no conflict of interest.

¹D.K. and M.M.R. contributed equally to this work.

²To whom correspondence may be addressed. E-mail: ajbard@mail.utexas.edu or mwhiteley@mail.utexas.edu.

This article contains supporting information online at www.pnas.org/lookup/suppl/doi:10.1073/pnas.1117298108/-DCSupplemental.

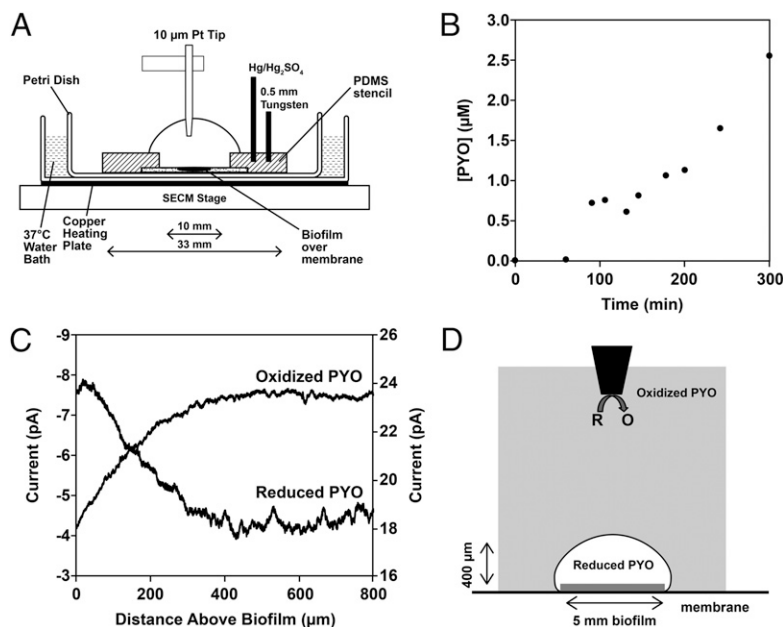


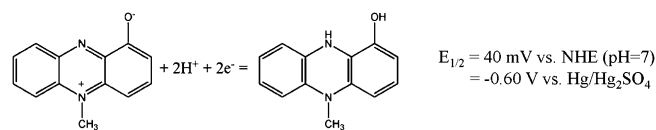
Fig. 1. (A) Schematic diagram of the SECM apparatus. (B) Real-time quantitative detection of PYO produced by a *P. aeruginosa* biofilm at 36 °C. (C) Z-direction reduced and oxidized PYO profiles at 36 °C. Zero on the x axis represents the surface of biofilm. (D) Proposed schematic model of PYO electrocline formation above a biofilm. To spatially map the reduced and oxidized PYO profile, the tip was biased at -0.3 V (oxidizing potential) and -0.8 V (reducing potential), respectively.

a virulence factor important for *P. aeruginosa* pathogenesis (28, 29). Our data reveal that *P. aeruginosa* biofilms produce high levels of PYO that is actively maintained in the reduced state proximal to the biofilm. This results in a reduced layer of PYO that we have termed the PYO “electrocline” (i.e., a gradient of redox potential), which extends several hundred microns away from the biofilm surface. We also demonstrate that the PYO electrocline is formed under electron acceptor-limiting conditions and that growth conditions favoring formation of the PYO electrocline correlate to an increase in soluble iron.

Results

Real-Time Quantitative Detection of PYO. We first sought to measure PYO concentrations directly above *P. aeruginosa* colony biofilms by using a unique biofilm SECM apparatus (Fig. 1A). For these experiments, the supernatant above the biofilm was removed and replaced with fresh medium at the beginning of the experiment to establish baseline (no PYO) SECM readings (11, 30). For PYO quantification, peak current was obtained from square wave voltammetry (Fig. S1), a unique application of SECM, and converted to PYO concentration using a calibration curve (Fig. S2). PYO was not immediately produced by newly formed *P. aeruginosa* biofilms; however, after only 5 h, the local (20 μm above the biofilm surface) PYO concentration was ≈ 2.5 μM (Fig. 1B). The delay in PYO production was also observed in planktonic cells (Fig. S3) and is not surprising because it is QS controlled.

Spatial Mapping Reveals a PYO Electrocline. PYO can exist in a reduced or oxidized state, governed by the half reaction:



and the redox state of PYO has important implications for its biological activity (31). Indeed, reduced PYO displays significant

antimicrobial activity (27) and the ability to reduce insoluble Fe³⁺ to soluble Fe²⁺ (32), whereas the oxidized form can potentially function as an alternative electron acceptor (33, 34). Thus, to understand the biological function of PYO, it would be valuable not only to measure PYO concentration, but also the PYO redox state. SECM is an excellent tool for these experiments because it allows both redox states of PYO to be assessed in real-time by biasing the SECM tip at -0.3 V (oxidizing at tip) and -0.8 V (reducing at tip). Z-direction spatial mapping of the PYO redox ratio above the *P. aeruginosa* biofilm revealed that the concentration of reduced PYO increased steadily as the tip approached the biofilm surface (Fig. 1C). This increase in reduced PYO correlated with a decrease in oxidized PYO at the biofilm surface (Fig. 1C). We have termed this area, beginning at the surface of the biofilm and extending to ≈ 400 μm above the biofilm, the PYO electrocline because the redox status of PYO transitions to a more reduced state within this region (Fig. 1D).

Because *P. aeruginosa* continually produces PYO during the course of the experiment, it is not possible to determine whether the PYO electrocline is due to increased production of reduced PYO or reduction of extracellular PYO. To examine this question, biofilms of *P. aeruginosa* $\Delta phz1/2$, a strain unable to produce phenazines because of deletion of both *phz* biosynthetic operons (26), were grown in the presence of a biologically relevant amount of exogenous PYO (33). Z-direction spatial mapping of the PYO redox ratio above the *P. aeruginosa* $\Delta phz1/2$ biofilm revealed a PYO electrocline, indicating that biosynthesis of PYO is not required for electrocline formation (Fig. 2A). The height of the electrocline extended beyond 400 μm, and similar to the PYO electrocline formed by WT *P. aeruginosa*, cyclic voltammograms (Fig. S4) showed that nearly all PYO was in the reduced form at a distance of 100 μm above the biofilm. Based on the observation that *P. aeruginosa* $\Delta phz1/2$ formed an electrocline similar to WT *P. aeruginosa* in the presence of exogenous PYO, we chose to use this model system for the remaining experiments because utilization of a constant level of PYO provided greater sensitivity and reliability.

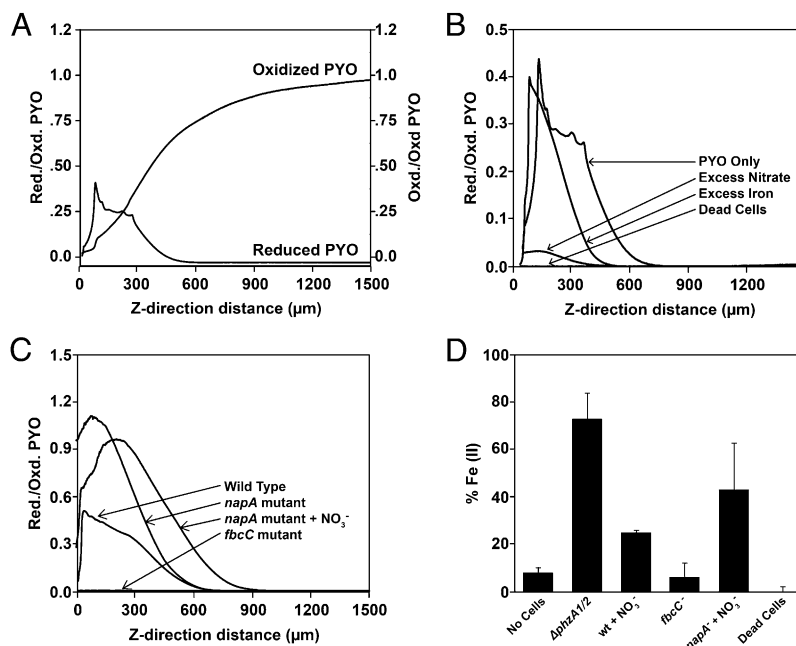


Fig. 2. (A) Z direction reduced and oxidized PYO profiles above a *P. aeruginosa* $\Delta phz1/2$ biofilm at 25 °C. (B) Z direction reduced PYO profiles above a *P. aeruginosa* $\Delta phz1/2$ biofilm in LB-MOPS (no addition) with 100 mM NO_3^- (excess nitrate), 100 μM Fe^{3+} (excess Fe^{3+}), or with heat killed cells (dead cells). (C) Z direction reduced PYO profiles above *P. aeruginosa* *napA* and *fbcC* mutants. (D) Measurement of Fe^{2+} in bulk solution in LB-MOPS (no cells), *P. aeruginosa* $\Delta phz1/2$ mutant biofilms in LB-MOPS, *P. aeruginosa* *fbcC* mutant in LB-MOPS, *P. aeruginosa* *napA* mutant in LB-MOPS with 100 mM NO_3^- (*napA*⁻ + NO_3^-), and a heat-killed *P. aeruginosa* biofilm (dead cells). In each case, 200 μM oxidized PYO was added to MOPS-LB growth medium. For A–C, the y axis was normalized to the concentration of oxidized PYO (200 μM) added to each biofilm.

It is important to note that for all PYO electroclines, a drop in PYO concentration is observed as the tip approaches closer than 60 μm of the biofilm surface. The reason for this drop is because when the tip is distal from the biofilm (i.e., >2,000 μm), the SECM instrument is operating in generation-collection mode but when the tip is within the electrocline, it switches to feedback mode. As a result, when the tip is proximal to the biofilm surface (i.e., within 60 μm), the response at the tip depends on how fast oxidized PYO at the tip is being reduced back by the biofilm. In these experiments, the rate of PYO reduction by the biofilm is not sufficient to exceed the rate of oxidation of PYO by the tip, hence the current drops at 60 μm or closer to the biofilm.

Determining the Mechanism of PYO Electrocline Development. Because PYO is proposed to serve as an alternative electron acceptor (33), we hypothesized that electrocline formation was due to the flow of electrons from carbon source oxidation to PYO. If this hypothesis is true, we predict that addition of another extracellular electron acceptor such as NO_3^- would reduce flux of electrons to PYO, thereby resulting in collapse of the PYO electrocline. To test this prediction, the impact of NO_3^- on the PYO electrocline produced by *P. aeruginosa* $\Delta phz1/2$ in the presence of exogenous PYO was assessed. As expected, in the presence of excess NO_3^- , the PYO electrocline collapsed (Fig. 2B). These data suggest that the presence of alternative electron acceptors is a critical parameter affecting the size of the PYO electrocline.

To definitively assess whether the collapse of the PYO electrocline was due to diversion of electron flux away from PYO to NO_3^- , the impact of NO_3^- on the PYO electrocline was assessed by using biofilms of a *P. aeruginosa* *napA* mutant. NapA is the periplasmic NO_3^- reductase important for reduction of NO_3^- under aerobic conditions (35); thus, the *P. aeruginosa* *napA* mutant is unable to divert electrons to NO_3^- under aerobic conditions. As expected, NO_3^- had no impact on the PYO electrocline in the *napA* mutant (Fig. 2C). In fact, the ratio of reduced/oxidized PYO within the electrocline almost doubled

for the *napA* mutant biofilm grown in the presence or absence of NO_3^- (Fig. 2C). This increase is likely due to reduction of trace amounts of NO_3^- present in our complex growth medium (35) by the WT *P. aeruginosa* biofilm. Collectively, these results indicate that the magnitude of the PYO electrocline is impacted by the presence of alternative electron acceptors. As a control for these experiments, the PYO electrocline produced by a *P. aeruginosa* *fbcC* mutant was also examined. FbcC is a subunit of cytochrome bc1, which has been reported to be the site at which PYO accepts electrons from aerobically growing *P. aeruginosa* (36). As expected for the *P. aeruginosa* *fbcC* mutant biofilm, the electrocline was almost completely abolished, confirming that this respiratory cytochrome is important for PYO electrocline formation (Fig. 2C).

Electrocline Formation Correlates with Fe^{2+} Enrichment. In addition to alternative electron acceptors, we predicted that exogenous molecules that actively facilitate reoxidation of PYO will also diminish the PYO electrocline. To test this prediction, the PYO electrocline was examined after addition of excess Fe^{3+} (100 μM , $\approx 10\times$ the concentration of the LB-MOPS growth medium). Fe^{3+} has been shown to oxidize PYO under aerobic conditions (32, 34). As expected, the PYO electrocline height decreased by 100 μm in the presence of excess Fe^{3+} ; however, the ratio of reduced/oxidized PYO within the electrocline remained the same. Based on these data, we hypothesized that a PYO electrocline may enrich the local environment around a biofilm with bioavailable Fe^{2+} even in the presence of oxygen. Using a Ferrozine-based Fe(II) assay (37), we measured Fe^{2+} from media exposed to colony biofilms for 1 h. Interestingly, Fe^{2+} levels increase under PYO electrocline forming conditions (Fig. 2D), whereas conditions that collapse the electrocline (NO_3^- addition or inactivation of cytochrome bc1) abrogate this increase in Fe^{2+} levels. Together, these data support a model in which metabolically active cells generate a reduced PYO electrocline, which subsequently serves as an electron donor to increase the ratio of Fe^{2+}/Fe^{3+} .

Electrochemical Imaging of a *P. aeruginosa* Biofilm. In addition to detailed spatial characterization of the PYO electrocline, the ability of *P. aeruginosa* biofilms to rapidly reduce oxidized PYO generated at the ultramicroelectrode tip indicated that SECM could also be used to generate a redox activity map of the biofilm surface. For these experiments, an SECM image of a 1-mm diameter *P. aeruginosa* Δ phz1/2 biofilm was performed at a constant height above the biofilm in the presence of exogenous PYO (Fig. 3). The tip was held at -0.3 V (PYO oxidizing potential) while scanning over the biofilm at a distance of 20–30 μ m from the biofilm surface maintaining a constant speed of 8 μ m/0.02 s. The false color contrast of the electrochemical image shows reactivity mapping of the biofilm as it reduces PYO that was oxidized by the SECM tip just above the biofilm (Fig. 3). The oxidized PYO diffused in the gap (tip-biofilm) where it was bacterially reduced resulting in higher current (red color) recorded by the tip (Fig. 3). Thus, the image can be seen as mapping of electron transfer from the biofilm to PYO, thereby providing a real-time examination of the PYO reducing ability of the biofilm. Biofilm redox mapping is an intriguing application for SECM and provides proof of principle that the redox activity of a biofilm, a strong indicator of metabolic activity, can be determined spatially in real-time.

Discussion

Bacteria in nature often reside in small, high-density sessile biofilms, and these small populations exhibit high-density signal-dependent phenotypes (38). Thus, the ability to determine small molecule concentrations in 3D space surrounding a biofilm in real-time will not only provide important insight into signal/cue levels proximal to bacterial clusters or biofilms, but will also provide new avenues for probing how biofilm spatial structure impacts small molecule perception and response by neighboring microbial communities.

Our laboratories previously adapted SECM to acquire quantitative data detailing metabolite concentration heterogeneity surrounding a biofilm (24). These initial studies led us to expand the utility of SECM not only to quantify the concentration of the signal/cue PYO, but also to noninvasively determine the redox status of biofilm-produced small molecules in 3D space. In this study, we demonstrate the utility of SECM to determine the concentration (Fig. 1B) and redox state of PYO (Fig. 1C), in real time, surrounding a biofilm—properties unable to be precisely

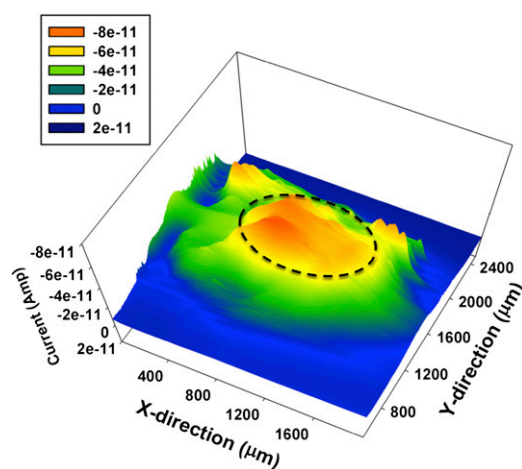


Fig. 3. A constant height SECM reactive image: of a 1-mm *P. aeruginosa* biofilm. Colors represent the current measured by SECM and correlates to the rate of PYO reduction by the biofilm from low (blue) to high current (red). A 2D scan was acquired by moving the SECM tip in the x and y axis at a fixed height (20–30 μ m) for the tip-substrate (biofilm) distance. The SECM tip was held at -0.3 V to oxidize PYO. Solution used: 200 μ M oxidized PYO in MOPS-LB. Dotted line indicates approximate size and position of the biofilm.

quantified by using other technologies. We also developed an application of square wave voltammetry (SWV) to detect PYO-dependent current as low as ≈ 0.7 pA (equivalent to ≈ 0.6 μ M PYO) (Fig. S1). Using spatial mapping in the z axis above the biofilm surface, we discovered the presence of a PYO electrocline proximal to the biofilm and demonstrate that this electrocline extends over 400 μ m from the biofilm surface (Figs. 1C and 2A).

To explain electrocline formation, we propose intracellular (Fig. 4A) and extracellular models (Fig. 4B), which occur in unison. Fig. 4A shows electron flow from carbon source oxidation to extracellular oxygen via NAD^+/NADH , the ubiquinone pool, and cytochrome bc1. When excess NO_3^- is present in the extracellular environment, electron flow is diverted from ubiquinone to reduce NO_3^- to NO_2^- through the NapA nitrate reductase (Fig. 4A). When PYO is present, electron flow is diverted from cytochrome bc1 to PYO instead of oxygen (Fig. 4A). Hence, we hypothesized that electrocline formation would be diminished by obstructing the electron flow either through cytochrome bc1 or by diverting electrons from the ubiquinone pool to the NapA nitrate reductase (Fig. 2B and C). In both cases, diversion of electron flow to PYO led to smaller PYO electroclines (Fig. 2B and C). In addition, an increased electrocline was observed for a *napA* mutant even in the presence of NO_3^- , likely due to additional electron flow to cytochrome bc1 as a result of electron flow divergence from inactivated NapA.

Modulation of the PYO electrocline height also depends on the concentration and redox state of iron (Fig. 4B). According to this model, the amount of reduced/oxidized PYO solely depends on k_f or the rate of electron transfer from the biofilm to the outside solution, whereas the height of an electrocline above a biofilm depends on the kinetic balance of k_1 , k_2 , and k_3 (see Fig. 4B for details). To maintain a PYO electrocline, the kinetics of electron transfer from the biofilm to PYO (k_f) must be greater than the kinetics of electron transfer from PYO to oxygen (k_1) and Fe^{3+} (k_2 and k_3). Reduced PYO reacts more readily with molecular oxygen than Fe^{3+} (34); thus, oxygen concentration proximal (≈ 400 μ m) to the biofilm decreases because of respiration and PYO-dependent oxygen reduction. Decrease in oxygen concentration has been demonstrated by PYO cyclic voltammogram data at 100 and 1,500 μ m above the biofilm (Fig. S4). Despite the presence of oxygen, PYO can also reduce Fe^{3+} to Fe^{2+} at pH 7 (32, 34). Therefore, we hypothesized that the addition of Fe^{3+} to the solution might play a role in modulating electrocline height by affecting k_2 . Fig. 2B supports this hypothesis showing that a decrease in height of the PYO electrocline is observed upon increasing Fe^{3+} concentration. Because electrocline formation correlates with an increase in soluble Fe^{2+} (Fig. 2D), we propose that an additional role for PYO is to scavenge iron near the biofilm surface by reduction of Fe^{3+} via a PYO electrocline. Modulation of electrocline height based on Fe^{3+} concentration could serve as a mechanism to expand an Fe-reducing electrocline when Fe^{3+} concentrations are low. This ability of PYO to enrich Fe^{2+} in areas immediately adjacent to the biofilm may provide *P. aeruginosa* with a means of obtaining soluble Fe^{2+} instead of relying on energy intensive siderophore-based Fe^{3+} transport mechanisms. Considering that iron is limiting in numerous environments including the human body, the role of the PYO electrocline in iron acquisition may have implications in disease. Based on recent studies, these observations may also extend to other *P. aeruginosa* phenazines (39).

The measurement of metabolite concentrations in 3D space above a bacterial biofilm has yielded the discovery of a redox electrocline generated by electron transport to a soluble small molecule. In addition to characterizing electrocline formation, we have also obtained a “reactive image” of a bacterial biofilm (Fig. 3), demonstrating the rate of bacterial redox activity across a 2D surface. These findings demonstrate a paradigm for metabolite measurement and present the possibility that electroclines and

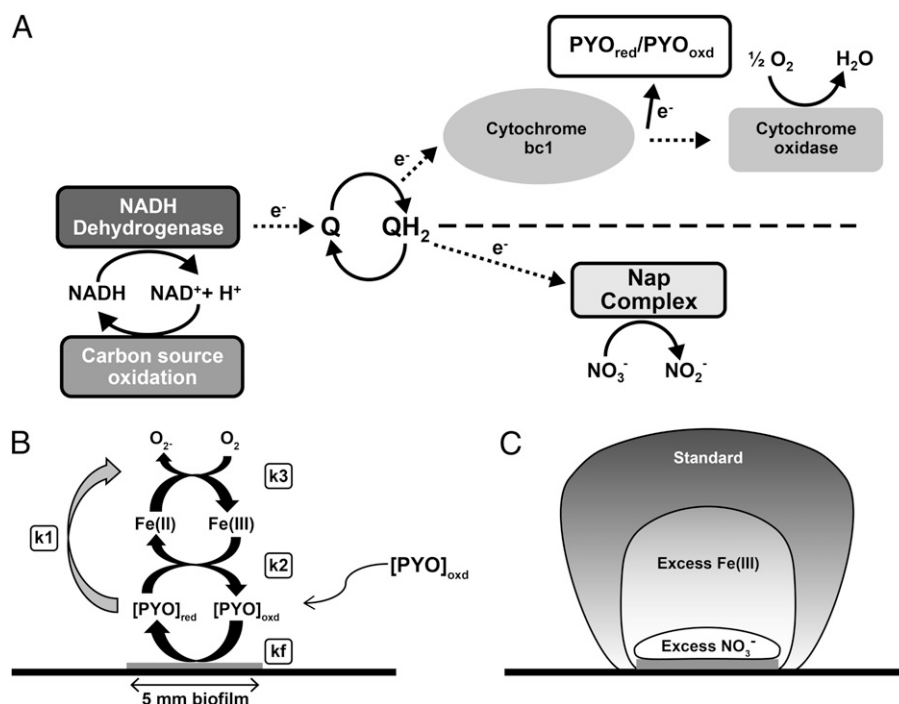


Fig. 4. (A) A schematic diagram of the proposed intracellular model of electron flow from carbon source oxidation to extracellular oxygen, PYO or NO₃⁻. Dotted arrows indicate abbreviated or unknown electron transport steps; solid arrows indicate direct electron transfer. (B) A schematic diagram of extracellular electron flow. K_f, heterogeneous electron transfer from biofilm to solution; k₁, rate of reaction between reduced PYO and molecular oxygen; k₂, rate of reaction between reduced PYO and Fe³⁺; k₃, rate of reaction between Fe²⁺ and oxygen. (C) A schematic representation of the modulation of a PYO electrocline in response to different extracellular conditions.

potentially other chemoclines produced by biofilms might serve important biological roles such as nutrient acquisition.

Materials and Methods

Materials. All chemicals were used as purchased without any further purification. PYO and potassium ferrocyanide were purchased from Sigma Aldrich. Ten-micrometer Pt wire was purchased from Good fellow. Deionized water (18 MΩ) was used to prepare all solutions.

Bacteria Culture and Biofilm Sample Preparation. *P. aeruginosa* PA14 and isogenic mutants were obtained from the PA14 nonredundant transposon library (40). *P. aeruginosa* Δ*phz1/2* was generated (26) (See Table S1 for details). Growth medium for all SECM experiments was LB-MOPS at pH 7.2. LB-MOPS consists of a 1/1 (vol/vol) mixture of Luria Bertani Broth (5 g/L yeast extract, 10 g/L tryptone, and 10 g/L NaCl) and MOPS buffer (41). In select experiments, cell supernatants were added to biofilms. To generate supernatants, the *P. aeruginosa* Δ*phz1/2* was inoculated into 3 mL of LB-MOPS medium and grown overnight. The culture was then diluted in fresh LB-MOPS to an optical density at 600 nm (OD₆₀₀) of 1, and centrifuged in a 15-mL tube at 7,000 × g for 10 min at 25 °C. Supernatants were decanted and stored at 4 °C until used.

For biofilm formation, *P. aeruginosa* was grown planktonically overnight and resuspended to an OD₆₀₀ of 1. Five microliters of this suspension was added to the surface of a 25-mm polycarbonate membrane (Whatman no. 110606). Before inoculation, membranes were placed on a Petri dish containing LB agar. Membranes were then overlaid with a “stencil” made of Sylgard 184 PDMS (Dow Corning). PDMS stencils were fabricated by casting ≈1.5 mL of PDMS into a 35-mm Petri dish with a 5-mm OD tube positioned flush with the center bottom of the well. Once polymerized, the stencil was removed from the dish and the tubing was displaced, leaving a 5-mm opening for biofilms to form. After inoculation, biofilms were allowed to form overnight at 37 °C. Biofilms were then moved to room temperature where membranes were gently separated from the PDMS overlay. Films were transferred to the SECM apparatus and overlaid with ≈600 μL of LB-MOPS.

Electrochemical Measurements. All of the electrochemical measurements were acquired by using SECM (CHI 920C; CH Instruments). A 10-μm Pt electrode was

used as the SECM tip. Details about SECM tip fabrication could be found elsewhere (25). Tungsten wire (0.5 mm) and Hg/Hg₂SO₄ (Radiometer) was used as counter and reference electrode, respectively. All of the potentials henceforth mentioned here were referred vs. Hg/Hg₂SO₄ (+0.64 V vs. NHE).

Real-Time Quantitative Detection of PYO Using SECM. For details on the SECM experimental setup, see Fig. S5 and Fig. S6. The biofilm was gently washed twice with 500 μL of LB-MOPS. Tip-substrate (biofilm) distance was then fixed at 20 μm with the aid of a negative feedback approach curve by using 1 mM ferrocyanide as a redox mediator. Cells were washed three times with LB-MOPS to remove any ferrocyanide in the solution. Finally, 600 μL of supernatant from *P. aeruginosa* Δ*phz1/2* was added to the chamber. Supernatant was used to mimic the initial supernatant above the biofilm that had to be removed after the feedback approach curve. Background current using SWV was then measured above the biofilm by an SECM tip. Once the background current was stabilized, the temperature of the water bath surrounding the Petri dish holding each sample was increased to 36 °C by using a copper heating plate connected to a Variac power supply. The temperature was constantly monitored by a thermocouple located outside the Petri dish. The time was set to zero when the temperature reached 36 °C. LB-MOPS (200 μL) was added to the chamber after 1.5 h to compensate for water loss due to evaporation. SWV was recorded at every 10 min until 5 h in the potential range of -0.35 to -0.85 V.

Once the background was recorded, PYO was added to the LB-MOPS covering the biofilm to a biologically relevant final concentration of 200 μM (33). After 30 min at 25 °C, the SECM tip was biased at -0.3 V (oxidizing reduced PYO at tip) and then moved in the z direction toward the biofilm from 2,000 μm away at the speed of 5 μm/s. Similarly, the tip was biased at -0.8 V (reducing oxidized PYO at tip) to map the z direction oxidized PYO profile above the biofilm.

Electrochemical Imaging of a Biofilm Using SECM. A 1-mm *P. aeruginosa* biofilm was used for SECM electrochemical imaging. The biofilm was grown and assembled on the SECM stage as described. The SECM stage tilt was fixed by performing a negative feedback approach curve using ferrocyanide as a redox mediator. PYO was then added to 500 μL of LB-MOPS to prepare a 200 μM PYO solution. A feedback mode SECM image of a wild-type biofilm was acquired at 25 °C by biasing the tip at -0.3 V. The tip-substrate (biofilm)

distance was kept constant at 20 μm (approximately). Scanning speed was maintained at 8 $\mu\text{m}/0.02$ s.

- Diggle SP, Gardner A, West SA, Griffin AS (2007) Evolutionary theory of bacterial quorum sensing: When is a signal not a signal? *Philos Trans R Soc Lond B Biol Sci* 362: 1241–1249.
- Fuqua WC, Winans SC, Greenberg EP (1994) Quorum sensing in bacteria: The LuxR-LuxI family of cell density-responsive transcriptional regulators. *J Bacteriol* 176: 269–275.
- Norman RS, Moeller P, McDonald TJ, Morris PJ (2004) Effect of pyocyanin on a crude-oil-degrading microbial community. *Appl Environ Microbiol* 70:4004–4011.
- Ramsey MM, Rumbaugh KP, Whiteley M (2011) Metabolite cross-feeding enhances virulence in a model polymicrobial infection. *PLoS Pathog* 7:e1002012.
- Ramsey MM, Whiteley M (2009) Polymicrobial interactions stimulate resistance to host innate immunity through metabolite perception. *Proc Natl Acad Sci USA* 106: 1578–1583.
- Price-Whelan A, Dietrich LE, Newman DK (2006) Rethinking ‘secondary’ metabolism: Physiological roles for phenazine antibiotics. *Nat Chem Biol* 2:71–78.
- Schertzer JW, Boulette ML, Whiteley M (2009) More than a signal: Non-signaling properties of quorum sensing molecules. *Trends Microbiol* 17:189–195.
- Kuspa A, Plamann L, Kaiser D (1992) A-signalling and the cell density requirement for *Myxococcus xanthus* development. *J Bacteriol* 174:7360–7369.
- Bainton NJ, et al. (1992) N-(3-oxohexanoyl)-L-homoserine lactone regulates carbenem antibiotic production in *Erwinia carotovora*. *Biochem J* 288:997–1004.
- Duerkop BA, et al. (2009) Quorum-sensing control of antibiotic synthesis in *Burkholderia thailandensis*. *J Bacteriol* 191:3909–3918.
- Latifi A, et al. (1995) Multiple homologues of LuxR and LuxI control expression of virulence determinants and secondary metabolites through quorum sensing in *Pseudomonas aeruginosa* PAO1. *Mol Microbiol* 17:333–343.
- Piersen LS, 3rd, Keppenne VD, Wood DW (1994) Phenazine antibiotic biosynthesis in *Pseudomonas aureofaciens* 30-84 is regulated by PhzR in response to cell density. *J Bacteriol* 176:3966–3974.
- Eberhard A, et al. (1981) Structural identification of autoinducer of *Photobacterium fischeri* luciferase. *Biochemistry* 20:2444–2449.
- Nealson KH, Platt T, Hastings JW (1970) Cellular control of the synthesis and activity of the bacterial luminescent system. *J Bacteriol* 104:313–322.
- Pearson JP, Feldman M, Iglewski BH, Prince A (2000) *Pseudomonas aeruginosa* cell-to-cell signaling is required for virulence in a model of acute pulmonary infection. *Infect Immun* 68:4331–4334.
- Costerton JW, Stewart PS, Greenberg EP (1999) Bacterial biofilms: A common cause of persistent infections. *Science* 284:1318–1322.
- Stewart PS, Franklin MJ (2008) Physiological heterogeneity in biofilms. *Nat Rev Microbiol* 6:199–210.
- Xu KD, Stewart PS, Xia F, Huang CT, McFeters GA (1998) Spatial physiological heterogeneity in *Pseudomonas aeruginosa* biofilm is determined by oxygen availability. *Appl Environ Microbiol* 64:4035–4039.
- Boles BR, Thoendel M, Singh PK (2004) Self-generated diversity produces “insurance effects” in biofilm communities. *Proc Natl Acad Sci USA* 101:16630–16635.
- Borriello G, et al. (2004) Oxygen limitation contributes to antibiotic tolerance of *Pseudomonas aeruginosa* in biofilms. *Antimicrob Agents Chemother* 48:2659–2664.
- Hidalgo G, et al. (2009) Functional tomographic fluorescence imaging of pH micro-environments in microbial biofilms by use of silica nanoparticle sensors. *Appl Environ Microbiol* 75:7426–7435.
- Hu Z, et al. (2007) Spatial distributions of copper in microbial biofilms by scanning electrochemical microscopy. *Environ Sci Technol* 41:936–941.
- Vroom JM, et al. (1999) Depth penetration and detection of pH gradients in biofilms by two-photon excitation microscopy. *Appl Environ Microbiol* 65:3502–3511.
- Liu X, et al. (2011) Real-time mapping of a hydrogen peroxide concentration profile across a polymicrobial bacterial biofilm using scanning electrochemical microscopy. *Proc Natl Acad Sci USA* 108:2668–2673.
- Bard AJ, Mirkin MV (2001) *Scanning Electrochemical Microscopy* (Marcel Dekker, New York), p 650.
- Dietrich LE, Price-Whelan A, Petersen A, Whiteley M, Newman DK (2006) The phenazine pyocyanin is a terminal signalling factor in the quorum sensing network of *Pseudomonas aeruginosa*. *Mol Microbiol* 61:1308–1321.
- Hassan HM, Fridovich I (1980) Mechanism of the antibiotic action pyocyanine. *J Bacteriol* 141:156–163.
- Britigan BE, et al. (1992) Interaction of the *Pseudomonas aeruginosa* secretory products pyocyanin and pyochelin generates hydroxyl radical and causes synergistic damage to endothelial cells. Implications for *Pseudomonas*-associated tissue injury. *J Clin Invest* 90:2187–2196.
- Ran H, Hassett DJ, Lau GW (2003) Human targets of *Pseudomonas aeruginosa* pyocyanin. *Proc Natl Acad Sci USA* 100:14315–14320.
- Whiteley M, Lee KM, Greenberg EP (1999) Identification of genes controlled by quorum sensing in *Pseudomonas aeruginosa*. *Proc Natl Acad Sci USA* 96:13904–13909.
- Reszka KJ, O'Malley Y, McCormick ML, Denning GM, Britigan BE (2004) Oxidation of pyocyanin, a cytotoxic product from *Pseudomonas aeruginosa*, by microperoxidase 11 and hydrogen peroxide. *Free Radic Biol Med* 36:1448–1459.
- Cox CD (1986) Role of pyocyanin in the acquisition of iron from transferrin. *Infect Immun* 52:263–270.
- Price-Whelan A, Dietrich LE, Newman DK (2007) Pyocyanin alters redox homeostasis and carbon flux through central metabolic pathways in *Pseudomonas aeruginosa* PA14. *J Bacteriol* 189:6372–6381.
- Wang Y, Newman DK (2008) Redox reactions of phenazine antibiotics with ferric (hydr)oxides and molecular oxygen. *Environ Sci Technol* 42:2380–2386.
- Palmer KL, Brown SA, Whiteley M (2007) Membrane-bound nitrate reductase is required for anaerobic growth in cystic fibrosis sputum. *J Bacteriol* 189:4449–4455.
- Price-Whelan A (2009) Physiology and mechanisms of pyocyanin reduction in *Pseudomonas aeruginosa*. PhD dissertation (California Institute of Technology, Pasadena, CA).
- Viollier E, Inglett PW, Hunter K, Roychoudhury AN, Van Cappellen P (2000) The ferrozine method revisited: Fe(II)/Fe(III) determination in natural waters. *Appl Geochem* 15:785–790.
- Connell JL, et al. (2010) Probing prokaryotic social behaviors with bacterial “lobster traps”. *MBio* 1:e00202–e00210.
- Wang Y, et al. (2011) Phenazine-1-carboxylic acid promotes bacterial biofilm development via ferrous iron acquisition. *J Bacteriol* 193:3606–3617.
- Liberati NT, et al. (2006) An ordered, nonredundant library of *Pseudomonas aeruginosa* strain PA14 transposon insertion mutants. *Proc Natl Acad Sci USA* 103:2833–2838.
- Palmer KL, Mashburn LM, Singh PK, Whiteley M (2005) Cystic fibrosis sputum supports growth and cues key aspects of *Pseudomonas aeruginosa* physiology. *J Bacteriol* 187: 5267–5277.